A time domain algorithm for reflection of waves on a viscoelastically supported Timoshenko beam

Dag V.J. Billger
Division of Mechanics
Chalmers University of Technology
S-412 96 Göteborg, Sweden

David J.N. Wall
Department of Mathematics and Statistics
University of Canterbury, Christchurch
New Zealand

No. 155 July, 1997

A time domain algorithm for reflection of waves on a viscoelastically supported Timoshenko beam

Dag V.J. Billger* David J.N. Wall†

August 3, 1997

Abstract

This paper presents a time domain algorithm for solving the direct wave scattering problem for a Timoshenko beam. The beam is assumed to be made of a homogeneous material and to be restrained by a viscoelastic suspension of finite length. In the Timoshenko beam, the characteristic wave-fronts propagate with two distinct velocities. This implies that the equation satisfied by the reflection operator contains three separate families of characteristic curves. Furthermore, the equation is both temporally and spatially dependent due to the finite extent of the suspension. The mathematical problem this paper addresses is the construction of an algorithm to solve an associated partial integro-differential equation with three distinct wave-front velocities. The mathematical techniques that are developed are applicable to any set of matrix-valued, functional, first order equations appropriate for reflection kernels. Some numerical examples are presented in order to validate the algorithm.

1 Introduction

Wave splitting and invariant imbedding techniques as tools for solving linear one dimensional scattering problems in the time domain were introduced in [5, 8, 9, 12]. Since the development of these techniques in the early nineteen eighties they have been combined with the Green function technique [21, 23] and with propagator methods [18, 19, 20]. They have been applied to a large area of research, mostly concerning direct and inverse scattering in electrodynamics. Although, studies covering elastic [14, 27], viscoelastic problems [3, 10, 17] and thermal transport processes [30] have been conducted as well. Recently these methods have also been extended to nonlinear wave scattering problems [7, 22] and problems in which the materials age with time [1, 2]. Central to the understanding to the range of problems the wave splitting can be applied to are the ideas of Vogel [29], who elucidated the fact that the wave splitting techniques only have relevance to hyperbolic partial differential equations. For further background information on wave splitting and invariant imbedding techniques there is a slightly outdated overview of this area of research in [11].

Recently, time domain methods have been successfully used to study scattering of transient waves in the Timoshenko beam. A wave splitting of the Timoshenko beam equation was first found by Olsson and Kristensson [25]. This was a precursory study for both the direct and

*Division of Mechanics, Chalmers University of Technology, S-412 96 Göteborg, Sweden.
†Department of Mathematics & Statistics, University of Canterbury, Christchurch 1, New Zealand

inverse problems, involving flexural waves, in beams. The wave splitting was further studied in [16] where the free, homogeneous beam equation[1], was solved by using the Green function technique. In [6], the imbedding approach was used to obtain reflection and transmission operators for a inhomogeneous beam[2], which is subject to structural support in the form of viscoelastic damping. It was also shown, in this reference, that these operators have explicit integral representations; the kernels of these integral representations are the solutions of the reflection and the transmission equation, respectively. Folkow [15] has examined the inverse problem of recovering the damping properties, from knowledge of reflection boundary data, for an homogeneous beam supported on a semi-infinite viscoelastic structure. When the suspension is semi-infinite the reflection kernel is spatially invariant, and hence satisfies simpler equations than those which are studied here.

The present work concerns numerical solution of the spatially dependent reflection equation, for a homogeneous beam suspended on a viscoelastic structure of finite length. The viscoelasticity is characterised by constitutive relations, that involve the past history of deflection and rotation of the cross-section of the beam through memory functions of the suspension. A field that is incident on the suspended region partly scatters into a reflected field at the boundary of incidence. The reflected field has an integral representation through a convolution of the incident field with a reflection kernel, the later is determined by solving the reflection equation. The kernel depends only on the material properties of the beam and the viscoelastic suspension, not on the incident field. In the Timoshenko beam, the characteristic wave-fronts propagate with two distinct velocities. This implies that the reflection equation will contain three separate families of characteristic curves. Furthermore, this equation has both temporal and spatial dependence due to the finite extent of the suspension. The mathematical problem this paper addresses is the construction of an algorithm to solve a partial integro-differential equation with three distinct wave-front velocities.

As the reflection equation contains three distinct families of characteristic curves this imposes considerable numerical constraints on any numerical algorithm that is used to solve this equation. Similar reflection equations are found elsewhere in the literature. For example, Ayoubi [4] described direct and inverse time domain algorithms for hyperbolic systems of N components and Dougherty [14] studied scattering from a stratified elastic slab surrounded by elastic half spaces and arrived at a reflection equation involving three characteristic families. Further, it should be pointed out that Stewart [26] also encountered such a reflection equation, but referred to Dougherty for the numerical algorithm. The choice of computational molecule, for the numerical algorithm presented in this paper, was influenced by Ayoubi. However, the reflection equation treated here differs in that it contains convolutional matrix operators, while, in the previously cited references, the corresponding matrix operators are purely multiplicative. To the authors knowledge *no* previous numerical computations have been presented for the three-speed reflection equation.

Section 2 contains a review of the results in [6]. In Section 3 the results from the preceding section are specialised to a beam that is viscoelastically restrained by a finite suspension. Time discretisation of the reflection kernel is treated in Section 4. Section 5 presents a predictor-corrector procedure, based on the method of Euler and the trapezoidal rule, as an algorithm to solve the reflection equation. The algorithm includes the use of linear interpolation in

[1]By the term homogeneous beam we mean that the material parameters associated with the beam are *not* functions of the axial dimension of the beam. The term free implies that the beam is unsupported along its entire length.

[2]The material parameters of the beam vary along its axial dimension.

the spatial coordinate. Numerical results, for a direct scattering problem on the Timoshenko beam by the finite extent viscoelastic support and comparison with several limiting cases, are presented in Section 6. Some technicalities are collected in two appendices.

2 Preliminaries

The type of wave dynamics that are the concern of this paper are those of flexural motions in beams. Within the context of the linear theory of elasticity, it is impossible to carry out an exact analysis for a beam of general cross-sectional shape. For this reason a simpler model which approximates the behaviour of flexural motions must be used instead. In addition, the wave splitting techniques require the governing equation to be hyperbolic in order to obtain causal results. The Timoshenko beam theory provides a one-dimensional approximate description that combines these necessary features.

According to the Timoshenko beam theory [28], transient bending and shearing motion of a viscoelastically supported beam is governed by the equations

$$\begin{aligned} &\frac{\partial}{\partial z}\left(f_1\gamma\right) - f_1\chi_1(u) = \rho A\frac{\partial^2 u}{\partial t^2}, \\ &\frac{\partial}{\partial z}\left(f_2\frac{\partial \psi}{\partial z}\right) + f_1\gamma - f_2\chi_2(\psi) = \rho I\frac{\partial^2 \psi}{\partial t^2}, \end{aligned} \tag{2.1}$$

where $u(z,t)$, $\psi(z,t)$ and $\gamma(z,t)$ can be interpreted as the mean transverse deflection, the mean rotation and the mean shear angle of the cross section, respectively [13]. The longitudinal coordinate is represented by z; see Figure 1. The beam is supported by a suspension which will provide viscoelastic damping on both u and ψ. The viscoelastic damping is modelled by the operators χ_i. Explicit expressions for these operators will be given in Section 3.

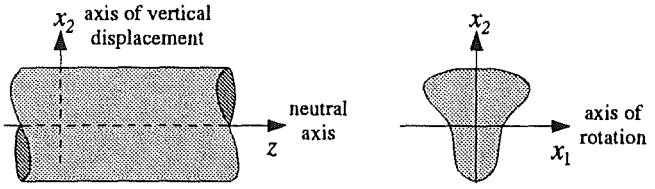

Figure 1: Axis definitions.

The material parameters appearing in (2.1) are the density ρ of the beam, the area of the cross section A and the moment of inertia I [3]. Furthermore, f_1 defines the shear stiffness and f_2 the bending stiffness through

$$f_1 = k'GA, \qquad f_2 = EI.$$

E and G are respectively, the modulus of elasticity, and the shear modulus, of the beam. Finally, k' is the shear coefficient which depends on the physical dimension of the cross

[3] In the case of a uniform beam the cross-section of the beam does not vary along the axial dimension of the beam. Therefore I, and A are not functions of z.

section and on the Poisson ratio ν; the later is defined from

$$\nu = \frac{E - 2G}{2G}, \qquad 0 \leq \nu < \frac{1}{2}.$$

The material of the beam is assumed incompressible with a non-negative Poisson's ratio, which imposes the limiting interval specified.

The flexural motions of the beam are characterised by two distinct wave-front velocities: the effective shear velocity, c_1, and the rod velocity, c_2. These are respectively defined by,

$$c_1 = \sqrt{\frac{f_1}{\rho A}}, \qquad c_2 = \sqrt{\frac{f_2}{\rho I}},$$

and they satisfy the inequality $c_2 > c_1$. The Timoshenko beam equation, (2.1), which governs these motions, can be written as a first order system by writing the dependent variables as

$$V = \begin{bmatrix} u & \psi & \gamma & \partial_z \psi \end{bmatrix}^T,$$

where γ and $\partial_z \psi$ are proportional to the shear force and the bending moment, and so can be respectively related as

$$\gamma = Q/f_1, \qquad \partial_z \psi = M/f_2. \tag{2.2}$$

The wave splitting is introduced by transforming this set of dependent variables into a new set U

$$U = \begin{bmatrix} u_1^+ & u_2^+ & u_1^- & u_2^- \end{bmatrix}^T,$$

by introducing a matrix-valued wave splitting operator $\mathcal{P}$ and its formal inverse $\mathcal{P}^{-1}$

$$U = \mathcal{P}V, \qquad V = \mathcal{P}^{-1}U. \tag{2.3}$$

The wave splitting transformation is defined by its property of diagonalising the Timoshenko beam equation in the homogeneous, unrestrained case. The splitting operator used throughout this paper is the one introduced in [16], which in turn is modified from the one initially introduced in [25]. The operators are collected in Appendix A of this paper; see in particular equations (A.5) and (A.6). The new set of dependent variables, are further ordered by

$$\boldsymbol{u}^+ = \begin{bmatrix} u_1^+ \\ u_2^+ \end{bmatrix}, \qquad \boldsymbol{u}^- = \begin{bmatrix} u_1^- \\ u_2^- \end{bmatrix},$$

which describe left- and right-moving vector fields, respectively. These fields are split in the sense that u_i^+ describes the right-moving field, while u_i^- describes the left-moving field. Moreover, the wave-fronts of the fields denoted by the subscript $i = 1$ propagate with the effective shear velocity c_1, and the wave-fronts corresponding to the subscript $i = 2$ propagate with the rod velocity c_2. In a homogeneous and unrestrained beam, the equations for the split fields are uncoupled. This is due to the diagonalising property of the chosen wave splitting transformation. If the beam is inhomogeneous over a region of compact support, then inside such a region, they couple, and the decomposition into left and right-moving fields is no longer possible. However, the wave splitting transformation remains a suitable mathematical tool

for studying the scattering of an incident field, from the homogeneous part of the beam, by a region of inhomogeneity. The reflected and transmitted fields are related to the incident field by reflection and transmission operators, which are independent of the incident field. These operators are described in [6].

The wave problem considered in this paper is that of scattering of a right-moving wave, in a homogeneous Timoshenko beam, by the region of the beam that resides on a viscoelastic suspension. The beam itself is homogeneous, and the only inhomogeneity in the equations is introduced by the finite support of the viscoelastic suspension; this is through the operators χ_i in (2.1) The length of this suspension is taken to be d, and the travel time of the faster wave-front in passing through this region then is d/c_2. In the sequel, non-dimensional space and time coordinates are introduced by means of the following travel time transformation

$$x(z) = \frac{z}{d}, \qquad s = \frac{c_2}{d}t.$$

Wherein z and t are the physical space and time coordinates, respectively. The domain of the scattering problem thus transforms into

$$\Omega = \{(x,s) : (x,s) \in [0,1] \times [0,\infty)\}.$$

In terms of the non-dimensional spatial variable, the inhomogeneous region of the beam is now confined to the interval $x \in [0,1]$. The beam is considered homogeneous outside of this region. If nothing further is stated, all fields in this paper are non-dimensional, and assumed quiescent at time $s < 0$. Non-dimensional temporal convolutions are denoted by a binary asterisk $(*)$

$$\mathbf{A} * \mathbf{B} = (\mathbf{A}(x,\cdot) * \mathbf{B}(x,\cdot))(s) = \int_0^s \mathbf{A}(x, s-s')\mathbf{B}(x,s')\,ds',$$

where $\mathbf{A}$ and $\mathbf{B}$ represent appropriate integrable 2-by-2 matrix-valued functions.

3 The imbedding equation for the reflection kernel

Consider the subregion $[x,1]$ of the full region of inhomogeneity $[0,1]$, for the suspension of the beam, as depicted in Figure 2. Then, with a fictitious replacement of the beam to the left of x by its homogeneous continuation, the scattering problem of the full region of inhomogeneity, $[0,1]$, can be imbedded in a family of scattering problems for each value of x for the subregions $[x,1]$. The relationship between the incident and reflected fields, at the left

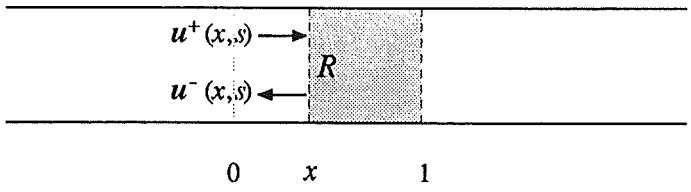

Figure 2: Uniform beam with a finite viscoelastic restraint.

boundary of subregion $[x,1]$, can be expressed by the temporal convolution

$$u^-(x,s) = \int_0^s \mathbf{R}(x, s-s')u^+(x,s')\,ds' = \mathbf{R} * u^+. \tag{3.1}$$

The reflection kernel of subregion $[x, 1]$, the 2-by-2 matrix $\mathbf{R}(x, s)$, is defined by the left going part of the impulse response of the scattering region, as evaluated at the left boundary x. Whereas the physical scattering kernel, for the suspension region $[0, 1]$, is $\mathbf{R}(0, s)$. The purpose of this imbedding is to convert the problem of equation (2.1) into an initial-boundary value problem for the reflection kernel.

In [6], the imbedding equation for the reflection kernel, along with its initial values and discontinuities, is derived. It has been found that this reflection kernel grows exponentially with time. In order to suppress any numerical instabilities that could otherwise occur, this exponential factor should be extracted in the numerical treatment of the reflection kernel. So it is desirable that the reflection kernel is transformed by extracting this exponential divergence, inherited from the wave splitting operator [16], by writing

$$\mathbf{R}'(x, s) = \exp(t/\tau)\mathbf{R}(x, s).$$

Here τ is a characteristic time parameter of the beam, defined in (A.2). Dropping the prime, the imbedding equation for the transformed reflection kernel can be shown to be

$$\partial_x \mathbf{R} - \mathbf{C}^{-1}\partial_s \mathbf{R} - \partial_s \mathbf{R}\,\mathbf{C}^{-1} = \mathcal{L}(\mathbf{R}) \quad \text{in} \quad \Omega, \tag{3.2}$$

where the terms involving derivatives on $\mathbf{R}$ have been collected on the left hand side of the equation, and the the right hand side is represented by the operator

$$\begin{aligned}\mathcal{L}(\mathbf{R}) = &\frac{d}{c_2\tau}\mathbf{C}\,\mathbf{R} + \frac{d}{c_2\tau}\mathbf{R}\,\mathbf{C} + \mathbf{F} * \mathbf{R} + \mathbf{R} * \mathbf{F} \\ &+ \mathbf{M}_{21} - \mathbf{M}_{11} * \mathbf{R} - \mathbf{R} * \mathbf{M}_{11} + \mathbf{R} * \mathbf{M}_{21} * \mathbf{R}.\end{aligned} \tag{3.3}$$

The initial values and boundary conditions, for this functional equation for $\mathbf{R}$, are homogeneous

$$R_{ij}(x, 0^+) = R_{ij}(1, s) = 0, \qquad i, j \in \{1, 2\}. \tag{3.4}$$

The matrices $\mathbf{C}$ and $\mathbf{F}$ in (3.2) and (3.3) can be expressed as

$$\mathbf{C} = \begin{bmatrix} c_1/c_2 & 0 \\ 0 & 1 \end{bmatrix}, \qquad \mathbf{F} = \left(\frac{d}{c_2\tau}\right)^2 e^{-ds/c_2\tau} \begin{bmatrix} F_1(s) & 0 \\ 0 & F_2(s) \end{bmatrix}, \tag{3.5}$$

where the F_i, $i \in \{1, 2\}$, are functions originating from the wave splitting and are defined in appendix A. It is also convenient to introduce the ratio of the effective shear velocity to the rod velocity, γ, as

$$\gamma = \frac{c_1}{c_2} < 1.$$

The 2-by-2 matrices $\mathbf{M}_{ij}$ can be defined in terms of matrix-valued operators, two known 2-by-2 matrix-valued time functions, as

$$\mathbf{M}_{11} = \chi_1(\mathbf{A}_1) + \chi_2(\mathbf{A}_2), \qquad \mathbf{M}_{21} = -\chi_1(\mathbf{A}_1) + \chi_2(\mathbf{A}_2). \tag{3.6}$$

These known functions $\mathbf{A}_1$ and $\mathbf{A}_2$ will be defined presently. The linear matrix-valued operators χ_i, $i \in \{1, 2\}$, contain the response functions and the spring constants of the viscoelastic suspension. The main contribution to the elastic part of the external forces is modelled by

spring constants k_1 and k_2. The viscoelastic part is modelled by convolution of $u(z,t)$ and $\psi(z,t)$ with response functions $K_1(t)$ and $K_2(t)$. These functions will also contribute to the elastic part of the response. The model taken for the χ_i operators is

$$\big(\chi_i(\mathbf{A})\big)_{lm} = \frac{d^2}{f_i}\big(k_i \mathbf{A}_{lm} + \widetilde{K}_i * \mathbf{A}_{lm}\big), \qquad i,l,m \in \{1,2\}, \tag{3.7}$$

where the subscript lm denotes the l-th row and k-th column of the matrix. In (3.7) the scalar convolution operator $\widetilde{K}_i$ is defined through

$$\big(\widetilde{K}_i * v\big)(s) = \frac{d}{c_2}\int_0^s e^{-(s-s')d/\tau c_2} K_i(s-s')v(s')\,ds', \qquad i \in \{1,2\}. \tag{3.8}$$

Furthermore, the matrices $\mathbf{A}_i$ are defined in terms of the time varying elements $A_{ij}(s)$, $i,j \in \{1,2\}$,

$$\mathbf{A}_1 = \begin{bmatrix} A_{11} & A_{11} \\ -A_{12} & -A_{12} \end{bmatrix}, \qquad \mathbf{A}_2 = \begin{bmatrix} -A_{21} & -A_{22} \\ A_{21} & A_{22} \end{bmatrix}, \tag{3.9}$$

which are given functional representation in Appendix A.

In the case of a homogeneous beam on a viscoelastic suspension, the reflection kernel $\mathbf{R}(x,s)$ is continuous everywhere in its domain [6]. However, there are discontinuities in the derivatives of the reflection kernel across the characteristic traces emanating from the point $(1,0)$. As a consequence of the fact that the wave-front velocities are constant, the characteristics are straight, and this is illustrated in Figure 3. The functions $d_m(x)$, which

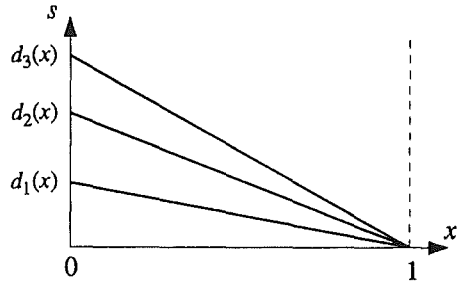

Figure 3: The characteristic traces across which the derivatives of the reflection kernel are discontinuous.

define the lines of discontinuity in the (x,s)-plane, are given by

$$d_1(x) = 2(1-x), \qquad d_2(x) = (1+\frac{1}{\gamma})(1-x), \qquad d_3(x) = \frac{2}{\gamma}(1-x). \tag{3.10}$$

The direct problem is to solve the well-posed system (3.2) for the reflection kernel $\mathbf{R}$, with the wave speed matrix $\mathbf{C}$ and the matrices $\mathbf{F}$, $\mathbf{M}_{11}$, and $\mathbf{M}_{21}$ being known. For convenience

in the next section, the component form of the matrix equation (3.2) is introduced

$$\begin{aligned}
\partial_x R_{11} - \frac{2}{\gamma}\partial_s R_{11} &= \mathcal{L}_{11}, \\
\partial_x R_{12} - \left(1+\frac{1}{\gamma}\right)\partial_s R_{12} &= \mathcal{L}_{12}, \\
\partial_x R_{21} - \left(1+\frac{1}{\gamma}\right)\partial_s R_{21} &= \mathcal{L}_{21}, \\
\partial_x R_{22} - 2\partial_s R_{22} &= \mathcal{L}_{22},
\end{aligned} \tag{3.11}$$

where $\mathcal{L}_{ij}$ denotes the elements of $\mathcal{L}(\mathbf{R})$, as given by (3.3).

4 Discretisation of the reflection equation

The system of equations (3.11) can be written in the abbreviated form

$$(\partial_x - \gamma_m \partial_s) R_{ij}(x,s) = \mathcal{L}_{ij}(x,s), \qquad i,j \in \{1,2\}, \tag{4.1}$$

where $m=1$ corresponds to $ij=22$, $m=2$ to $ij \in \{12,21\}$ and $m=3$ to $ij=11$, and with

$$\gamma_1 = 2, \qquad \gamma_2 = 1+\frac{1}{\gamma}, \qquad \gamma_3 = \frac{2}{\gamma}.$$

Equation (4.1) constitutes a semi-linear system of coupled, integro-differential equations for the direct problem.

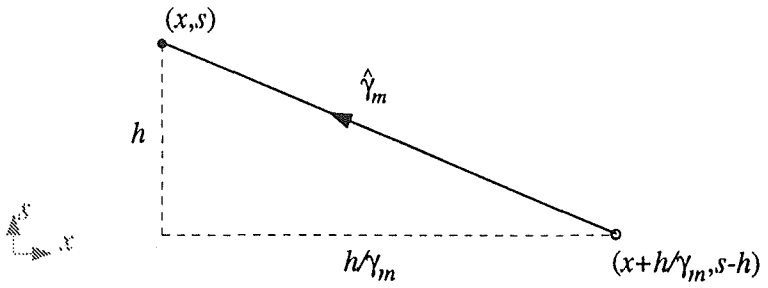

Figure 4: A time increment of the m-th characteristic.

The rewriting of the partial derivatives on the left hand side of (4.1), as directional derivatives along the directions of the appropriate characteristic traces (see Figure 4), results in the characteristic form of (4.1). The characteristic form is

$$D_m R_{ij}(x,s) = -\frac{1}{\sqrt{1+\gamma_m^2}}\mathcal{L}_{ij}(x,s), \tag{4.2}$$

where D_m denotes the directional derivative in the direction of the unit vector $\hat{\gamma}_m = (-1,\gamma_m)/(1+\gamma_m^2)^{1/2}$. Numerical solution of the system (4.2), by finite difference methods, requires approximation of the directional derivatives and the convolutions, contained in the operator of the right hand side. To this end, the time variable is discretised with a constant step size h

$$s_k = kh, \qquad k = 0,1,2,\ldots$$

Local approximation of the directional derivatives in (4.2), over small time increments of the respective characteristics, then gives

$$R_{ij}(x, s_k) = R_{ij}(x + h/\gamma_m, s_{k-1}) - \frac{h}{\gamma_m}\mathcal{L}_{ij}(x + h/\gamma_m, s_{k-1}) + \mathcal{O}(h^2), \qquad k \in \mathbb{Z}_+, \tag{4.3}$$

where $\mathbb{Z}_+$ denotes the positive integers. This is Euler's method. The resulting equation is an *explicit* equation providing $R_{ij}(x, s_k)$, in terms of earlier time values $R_{ij}(x+h/\gamma_m, s_{k-1})$, with a consistency error of $\mathcal{O}(h)$ [24]. Alternatively, direct integration of (4.2) with subsequent approximation of the resulting integral by the trapezoidal quadrature rule, results in

$$R_{ij}(x, s_k) = R_{ij}(x + h/\gamma_m, s_{k-1}) - \frac{h}{2\gamma_m}\big(\mathcal{L}_{ij}(x, s_k) + \mathcal{L}_{ij}(x + h/\gamma_m, s_{k-1})\big) + \mathcal{O}(h^3). \tag{4.4}$$

If $\mathcal{L}(\mathbf{R})$ is a non-linear operator, the resulting equation is an *implicit* equation for $R_{ij}(x, s_k)$, having a consistency error of $\mathcal{O}(h^2)$. In Section 5, these two methods are combined into an iterative method of solution.

The $\mathcal{L}(\mathbf{R})$ operator couples the elements $R_{ij}(x, s')$ linearly for all times $s' \in [0, s]$, with x fixed, because of the temporal convolutions. Therefore, for notational simplicity, the x-dependence of the operator will be suppressed in the remaining part of this section. The notation used for the time discretisation of the matrices constituting $\mathcal{L}(\mathbf{R})$ is

$$\mathbf{R}(x, s_k) = \mathbf{R}_k, \qquad \mathbf{F}(s_k) = \mathbf{F}_k, \qquad \mathbf{M}_{11}(s_k) = \mathbf{M}_{11,k}, \qquad \mathbf{M}_{21}(s_k) = \mathbf{M}_{21,k}.$$

Also, for convenience, the anti-commutator bracket is introduced to denote the symmetric sum of matrix products

$$\{\mathbf{A}, \mathbf{B}\} = \mathbf{AB} + \mathbf{BA}. \tag{4.5}$$

The temporal convolutions in $\mathcal{L}(\mathbf{R})$ are approximated by the trapezoidal quadrature rule using a uniform time step h. General expressions for such convolutions are given in appendix B. By causality of $\mathbf{R}$, and the initial conditions (3.4), the convolutions containing the matrix $\mathbf{M}_{11}$ are approximated as follows

$$\big(\mathbf{M}_{11} * \mathbf{R}\big)_k + \big(\mathbf{R} * \mathbf{M}_{11}\big)_k = h \sum_{p=0}^{k-1}{}' \left\{\mathbf{M}_{11,p}, \mathbf{R}_{k-p}\right\}, \tag{4.6}$$

where the single prime on the summation symbol signifies that the first term in the summation is to be halved. The convolutions containing $\mathbf{F}$ can likewise be approximated as

$$\big(\mathbf{F} * \mathbf{R}\big)_k + \big(\mathbf{R} * \mathbf{F}\big)_k = h \sum_{p=0}^{k-1}{}' \left\{\mathbf{F}_p, \mathbf{R}_{k-p}\right\}. \tag{4.7}$$

Finally, the double convolution containing $\mathbf{M}_{21}$ has the approximation

$$(\mathbf{R} * \mathbf{M}_{21} * \mathbf{R})_k = h^2 \sum_{p=1}^{k-1} \left(\sum_{q=1}^{p} \mathbf{R}_q \mathbf{M}_{21,p-q} - \frac{1}{2}\mathbf{R}_p \mathbf{M}_{21,0} \right) \mathbf{R}_{k-p}. \tag{4.8}$$

The standard usage is to be taken when the lower limit of the sum in either (4.6), (4.7) or (4.8) equals, or exceeds, the upper limit, the contribution of that sum is zero.

The time discretised form of $\mathcal{L}(\mathbf{R})$, with a discretisation error of $\mathcal{O}(h^2)$, can now be written

$$[\mathcal{L}(\mathbf{R})]_k = \left\{ \frac{d}{c_2\tau}\mathbf{C}^{-1} + \frac{h}{2}(\mathbf{F}_0 - \mathbf{M}_{11,0}), \mathbf{R}_k \right\} + [\mathcal{M}(\mathbf{R})]_k, \tag{4.9}$$

where

$$\begin{aligned}[\mathcal{M}(\mathbf{R})]_k = \mathbf{M}_{21,k} &+ h\sum_{p=1}^{k-1}\{\mathbf{F}_p - \mathbf{M}_{11,p}, \mathbf{R}_{k-p}\} \\ &+ h^2\sum_{p=1}^{k-1}\left(\sum_{q=1}^{p}\mathbf{R}_q\mathbf{M}_{21,p-q} - \frac{1}{2}\mathbf{R}_p\mathbf{M}_{21,0}\right)\mathbf{R}_{k-p}.\end{aligned} \tag{4.10}$$

In (4.9), $[\mathcal{L}(\mathbf{R})]_k$ has been subdivided into two parts. One part $[\mathcal{M}(\mathbf{R})]_k$ which depends only on past time values of $\mathbf{R}_p$, $0 < p \leq k-1$, and an extracted part that depends explicitly on $\mathbf{R}_k$. This means, when solving the system (4.4) for R_{ij}, that the extracted part alone accounts for the coupling of the system of equations at the point of calculation.

To analyse the convergence of the fixed point algorithm, for implementation of an implicit method of solution of equation (4.1), it is necessary to develop the coupling term explicitly. To this end, equation (4.9) indicates that in order to determine the coupling term, the matrices $\mathbf{F}$ and $\mathbf{M}$ must be calculated at time $s = 0^+$. These terms are listed from (3.5), (3.7) and (A.1)

$$\mathbf{F}_0 = \frac{d^2 f_1}{2f_2(1-\gamma^2)}\begin{bmatrix}-\gamma & 0\\ 0 & 1\end{bmatrix}, \qquad \chi_i(\mathbf{A})_0 = d^2\frac{k_i}{f_i}\mathbf{A}_0.$$

Furthermore, from (3.9) and (A.3),

$$\mathbf{A}_{1,0} = \frac{\gamma}{2}\begin{bmatrix}-1 & -1\\ 0 & 0\end{bmatrix}, \qquad \mathbf{A}_{2,0} = \frac{1}{2}\begin{bmatrix}0 & 1\\ 0 & -1\end{bmatrix},$$

and then from (3.6)

$$\mathbf{M}_{11,0} = \frac{d^2}{2}\begin{bmatrix}-\gamma\frac{k_1}{f_1} & \frac{k_2}{f_2} - \gamma\frac{k_1}{f_1}\\ 0 & -\frac{k_2}{f_2}\end{bmatrix}, \qquad \mathbf{M}_{21,0} = \frac{d^2}{2}\begin{bmatrix}\gamma\frac{k_1}{f_1} & \frac{k_2}{f_2} + \gamma\frac{k_1}{f_1}\\ 0 & -\frac{k_2}{f_2}\end{bmatrix}.$$

By introducing the coupling matrix

$$\Delta \equiv \frac{d}{c_2\tau}\mathbf{C}^{-1} + \frac{h}{2}(\mathbf{F}_0 - \mathbf{M}_{11,0}) = \begin{bmatrix}\Delta_1 & \Delta_2\\ 0 & \Delta_3\end{bmatrix},$$

where

$$\begin{aligned}\Delta_1 &= \frac{1}{\gamma}\frac{d}{c_2\tau} + \frac{d^2}{2}\left(\gamma\frac{k_1}{f_1} - \frac{\gamma}{1-\gamma^2}\frac{f_1}{f_2}\right)\frac{h}{2},\\ \Delta_2 &= \frac{d^2}{2}\left(\gamma\frac{k_1}{f_1} - \frac{k_2}{f_2}\right)\frac{h}{2},\\ \Delta_3 &= \frac{d}{c_2\tau} + \frac{d^2}{2}\left(\frac{k_2}{f_2} + \frac{1}{1-\gamma^2}\frac{f_1}{f_2}\right)\frac{h}{2},\end{aligned}$$

the coupling term can be given in explicit form

$$\{\boldsymbol{\Delta}, \mathbf{R}_k\} = \begin{bmatrix} 2\Delta_1 R_{11,k} + \Delta_2 R_{21,k} & \Delta_2(R_{11,k} + R_{22,k}) + (\Delta_1 + \Delta_3) R_{12,k} \\ (\Delta_1 + \Delta_3) R_{21,k} & 2\Delta_3 R_{22,k} + \Delta_2 R_{21,k} \end{bmatrix}.$$

5 Numerical algorithm

With the time discretisation of the system (4.2), an iterative procedure can be constructed for calculating $R_{ij}(x, s)$ from the known values at previous times. The computational molecule for the direct problem is shown in Figure 5. Note that the physical restrictions on the parameters (see equation (3.10)), ensure that the reciprocal of the slope of each characteristic trace satisfies

$$\gamma_1 < \gamma_2 < \gamma_3 \quad \text{for} \quad \gamma < 1.$$

This inequality is easily proved. It follows that the ordering of the characteristic traces in Figure 5 is always correct; this is important for the algorithm used. Past values of R_{ij}, at the time $s - h$, propagate along the characteristic traces, through the common time interval h, and coincide at the calculation point P. Thereby giving information about $R_{ij}(x, s)$ at the current time value s.

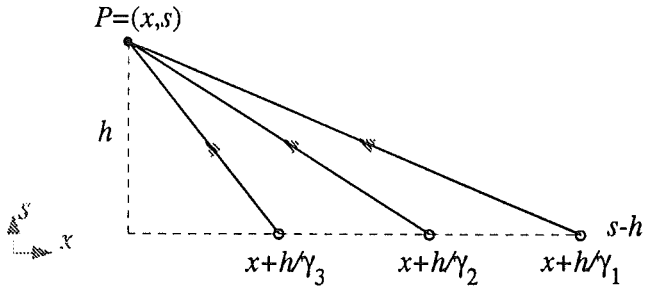

Figure 5: The computational molecule.

Following the notation, the time discretised matrix elements of equation (4.2) are denoted by

$$R_{ij}(x, s_k) = R_{ij}(x)_k, \qquad \mathcal{L}_{ij}(x, s_k) = \left[\mathcal{L}_{ij}(x)\right]_k.$$

Then the discretisation form (4.9), obtained in the preceding section, is in elemental form

$$\left[\mathcal{L}_{ij}(x)\right]_k = \{\boldsymbol{\Delta}, \mathbf{R}(x)_k\}_{ij} + \left[\mathcal{M}_{ij}(x)\right]_k.$$

Insertion of these expressions into both Euler's method (4.3), and the trapezoidal method (4.4), leads to the following fix point iteration formulae

$$R_{ij}(x)_k^{(0)} = R_{ij}(x + h/\gamma_m)_{k-1} - \frac{h}{\gamma_m}\left[\mathcal{L}_{ij}(x + h/\gamma_m)\right]_{k-1},$$

$$R_{ij}(x)_k^{(p+1)} = R_{ij}(x + h/\gamma_m)_{k-1} - \frac{h}{2\gamma_m}\left(\left[\mathcal{L}_{ij}(x + h/\gamma_m)\right]_{k-1} + \left[\mathcal{M}_{ij}(x)\right]_k\right) \tag{5.1}$$

$$- \frac{h}{2\gamma_m}\{\boldsymbol{\Delta}, \mathbf{R}(x)_k^{(p)}\}_{ij},$$

in which the superscript $p = 0, 1, 2, \ldots$ enumerates the iteration sequence for $R_{ij}(x)_k^{(p)}$ with both k and x fixed. This is a predictor-corrector procedure, in which Euler's method, the predictor, supplies a starting value for an iteration sequence which is generated by the trapezoidal rule, the corrector. For a sufficiently small time step, h, the corrector iteration will converge.

To estimate an upper limit of h the elements of the reflection matrix are rewritten as a column vector

$$\boldsymbol{r} = \left[= R_{11}(x)_k \quad R_{12}(x)_k \quad R_{21}(x)_k \quad R_{22}(x)_k\right]^T .$$

Then the predictor-corrector procedure of equation (5.1) can be rewritten as

$$\boldsymbol{r}^{(p)} = \boldsymbol{a} - \frac{h}{2}(\boldsymbol{b} + \boldsymbol{c}) - \frac{h}{2}\boldsymbol{T}\boldsymbol{r}^{(p-1)}, \qquad \boldsymbol{r}^{(0)} = \boldsymbol{a} - h\boldsymbol{b}, \qquad p \in \mathbb{Z}_+, \tag{5.2}$$

with the column vectors expressed as

$$\boldsymbol{a} = \begin{bmatrix} R_{11}(x + h/\gamma_3)_{k-1} \\ R_{12}(x + h/\gamma_2)_{k-1} \\ R_{21}(x + h/\gamma_2)_{k-1} \\ R_{22}(x + h/\gamma_1)_{k-1} \end{bmatrix}, \qquad \boldsymbol{b} = \begin{bmatrix} \frac{1}{\gamma_3}\mathcal{L}_{11}(x + h/\gamma_3)_{k-1} \\ \frac{1}{\gamma_2}\mathcal{L}_{12}(x + h/\gamma_2)_{k-1} \\ \frac{1}{\gamma_2}\mathcal{L}_{21}(x + h/\gamma_2)_{k-1} \\ \frac{1}{\gamma_1}\mathcal{L}_{22}(x + h/\gamma_1)_{k-1} \end{bmatrix}, \qquad \boldsymbol{c} = \begin{bmatrix} \frac{1}{\gamma_3}\mathcal{M}_{11}(x)_k \\ \frac{1}{\gamma_2}\mathcal{M}_{12}(x)_k \\ \frac{1}{\gamma_2}\mathcal{M}_{21}(x)_k \\ \frac{1}{\gamma_1}\mathcal{M}_{22}(x)_k \end{bmatrix}.$$

Finally, the matrix $\boldsymbol{T}$ contains the elements of the coupling matrix Δ, as

$$\boldsymbol{T} = \begin{bmatrix} \gamma\Delta_1 & 0 & \frac{\gamma}{2}\Delta_2 & 0 \\ \frac{\gamma}{1+\gamma}\Delta_2 & \frac{\gamma}{1+\gamma}(\Delta_1 + \Delta_3) & 0 & \frac{\gamma}{1+\gamma}\Delta_2 \\ 0 & 0 & \frac{\gamma}{1+\gamma}(\Delta_1 + \Delta_3) & 0 \\ 0 & 0 & \frac{1}{2}\Delta_2 & \Delta_3 \end{bmatrix}.$$

By the Banach fixed point theorem [24] a fixed point exists, and is unique, if $\boldsymbol{T}$ is a contraction mapping. This is the case when

$$\frac{h}{2}\|\boldsymbol{T}\| < 1,$$

with respect to an appropriate matrix norm. This is a convergence criterion for the iteration. Note that $\boldsymbol{T}$ is h-dependent. The equation (5.2) suggests another way of approaching the numerical solution of the reflection equation; the rewritten trapezoidal rule in (5.2) can be solved directly since $\boldsymbol{T}$ is independent of $\boldsymbol{r}$. However, this is rarely necessary and will not be pursued in the present paper.

One of the difficulties in solving the system (5.1) is the fact that propagation of information occurs along three distinct characteristics and that the reflection kernel may suffer from discontinuities in its derivatives across some of these characteristics. This means that the use of a completely uniform mesh structure would cause these discontinuities to diffuse. In the algorithm presented here, a uniform mesh is used as a base mesh and interpolation is used to calculate data at points which are not on the base mesh. Discontinuities may propagate along the three characteristic traces emanating from the point $(1, 0)$, (see Figure 6). Therefore, these traces must be kept track of in the algorithm, and no interpolation performed across them,

in order to avoid causing diffusion of the discontinuities. The interpolation chosen was linear, so that a discretisation error of $\mathcal{O}(h^2)$ is maintained.

To form the base mesh the spatial interval $x \in [0,1]$ is divided into N subintervals, *i.e.*

$$x_n = n/N, \qquad n = 0, 1, 2, \ldots, N.$$

The time step, h, of the corrector iteration is chosen so that the characteristic trace corresponding to the slowness $\gamma_1 = 2$ coincides with a node point in the mesh at every time step, this means

$$s_k = kh = 2k/N, \qquad k = 0, 1, 2, \ldots$$

The points of intersection of the remaining characteristic traces with each time step are added to the uniform base mesh; see the dots in Figure 6. These points are considered as being on the discontinuity characteristic traces since the reflection kernel is continuous. They are in general non-coincident with the base-mesh.

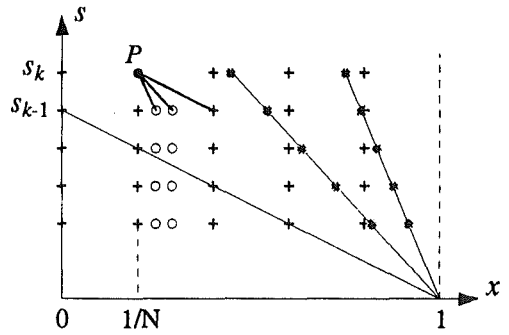

Figure 6: The uniform base mesh and the added points. The open circles are points of interpolation, the dots are added points and the crosses represent nodes of the mesh. The lines are the characteristic traces.

The scheme for calculation of the reflection kernel is as follows

Algorithm 1 *Calculation of the reflection kernel $R(x,s)$:*

1. Determine the kernel for all mesh nodes at s_1: *The initial conditions $R_{ij}(x)_{k=0} = 0$ are sequentially inserted into the predictor-corrector procedure* (5.1). *Thus the discrete set $\{R_{ij}(x_n)_{k=1}\}_{n=0}^{N}$ is obtained.*

2. Determine the kernel for the points of intersection at $s_1 = h$: *The reflection kernel is calculated at the off-node intersection points of the characteristics $d_1(x)$ and $d_2(x)$ with time $s_1 = h$.*

3. Determine the kernel for all off-node points at s_1: *The set $\{R_{ij}(x_n)_{k=1}\}_{n=0}^{N}$ is linearly interpolated, from the base mesh, to retrieve $R_{ij}(x)_{k=1}$ for all $x \in [0,1]$. In performing the linear interpolation, knowledge of the intersections of the discontinuity characteristic traces with the present time step, and the values of the reflection kernel at those points, is used to ensure that no interpolation is performed across a characteristic trace.*

s	r_1	r_2	r_3
1.04	4.01	4.19	5.02
1.12	4.01	4.19	5.00
1.20	4.01	4.19	4.99
1.28	4.01	4.19	5.01
1.36	4.01	4.19	5.00
1.44	4.01	4.19	5.01
1.52	4.01	4.19	5.00
1.60	4.02	4.19	5.00
1.68	4.02	4.19	5.00
1.76	4.02	4.19	5.01
1.84	4.02	4.19	5.00
1.92	4.02	4.20	5.01
2.00	4.02	4.20	4.99
2.08	4.02	4.19	5.01
2.16	4.02	4.19	5.00
2.24	4.02	4.19	4.99
2.32	4.02	4.20	5.00

Table 1: Convergence ratios, tabulated against time s, for 3 halvings of the timestep h of the reflection kernel $R_{11}(0,s)$.

4. Repeat procedure: *The iteration procedure is subsequently repeated to obtain the set* $\{R_{ij}(x_n)_{k=2}\}_{j=0}^{N}$, *which is in turn interpolated to give* $R_{ij}(x)_{k=2}$ *for all* $x \in [0,1]$. *Steps 2-4 of this scheme are then applied repeatedly until a pre-set final time has been reached.*

The discretisation error of the algorithm is now discussed, the discussion is formal and exact consideration of the algorithm is possible by considerations such as [31]. If the elements of the reflection kernel are two times continuously differentiable in the x coordinate, then the discretisation error introduced by the linear interpolation procedure is $\mathcal{O}(1/N^2)$. Furthermore, with the choice of mesh made above, the consistency of the corrector iteration is of order $h^2 = N^{-2}$. Therefore, the overall discretisation error in the algorithm is of the same order as that of the interpolation; namely $\mathcal{O}(h^2)$. If the location of the discontinuity characteristic traces is not accounted for in the algorithm, the global discretisation error will be $\mathcal{O}(h)$ and diffusion of the discontinuities will occur.

For notational convenience the value of $R_{ij}(x,s)$, obtained from the algorithm with a step size determined by N, is denoted R_N for fixed (x,s). The *exact* value of the reflection kernel,

at the same point of calculation (x, s), is denoted R. Then, the earlier discussion on the discretisation error implies that $R - R_N \approx c/N^p$, with $p = 2$. If this is correct it implies that

$$\frac{R_{2N} - R_N}{R_{4N} - R_{2N}} = \frac{(R - R_N) - (R - R_{2N})}{(R - R_{2N}) - (R - R_{4N})} \approx \frac{(c/N^p) - (c/2^p N^p)}{(c/2^p N^p) - (c/4^p N^p)} = 2^p,$$

so that calculation of the ratio

$$r_i = \frac{R_{i2N} - R_{iN}}{R_{i4N} - R_{i2N}}, \quad i \in \{1, 2, 3 \dots\},$$

provides a numerical estimate of p. If $p = 2$, the ratio will equal 4. If the method is only of $\mathcal{O}(h)$, the convergence ratio should be 2. Table 1 lists convergence ratios for R_{11}, at several values of N, evaluated at $(x, s) = (0, s)$. The table illustrates, by numerical experiment, that a discretisation error of $\mathcal{O}(h^2)$ is in fact being achieved.

At each node the elements $\left[\mathcal{M}_{ij}(x)\right]_k$ have to be calculated for both the present and the retarded time, which is obvious from (5.1). However, the elements calculated at the present time step can be saved and recycled in the next time step where they give the value at the retarded time. The off-node values are calculated by linear interpolation. The discretisation error introduced by this interpolation is $\mathcal{O}(h^2)$ in $\left[\mathcal{M}_{ij}(x)\right]_k$. Therefore, the convolutions in (4.10) only have to be performed once per node. Consequently, this speed-up technique does not affect the overall discretisation error of the algorithm.

6 Numerical results

In the numerical examples presented here, the material parameters relevant to the reflection equation were chosen to match those of a uniform beam of square cross section. All common parameters for the numerical examples are summarised in Table 2. The shear coefficient k' was chosen in accordance with [13]. The length of the viscoelastic suspension need not be explicitly stated, since only the ratio of the length to the width of the cross section enters into the equation. Non-dimensional forms of the spring constants and memory kernels are introduced by

$$k_i' = \frac{c_2^2 \tau^2}{f_i} k_i, \qquad K_i(s)' = \frac{c_2^2 \tau^3}{f_i} K_i(s).$$

The primes are henceforth dropped. In the examples that were considered, the viscoelastic damping was modelled by exponential memory kernels of the form $K_i(s) = -k_i e^{-s}$. The spring constants were taken to be the same in all examples, and are given in Table 2.

The wave scattering problem treated in this section will now be described. A beam, which is semi-infinite in the positive x-direction, resides on a viscoelastic suspension of support $x \in [1, 2]$. The left end of this interval will henceforth be referred to as the reflection boundary. The left end of the beam, at $x = 0$, is subjected to a temporal pulse in the shear force, while the rotational motion of the left end is restrained. The appropriate boundary conditions are therefore

$$Q(0, s) = \begin{cases} -\frac{1}{2} Q_0 & \text{for } 0 < s < 1 \\ 0 & \text{otherwise} \end{cases}, \tag{6.1}$$

$$\psi(0, s) = 0. \tag{6.2}$$

Poisson's ratio	$\nu = 0.3$
Shear coefficient	$k' = \frac{10(1+\nu)}{12+11\nu} = 0.85$
Velocity ratio	$\gamma = \sqrt{\frac{k'}{2(1+\nu)}} = 0.57$
Ratio of suspension length to beam width	$\frac{d}{a} = 0.30$
Spring constants	$k_1 = k_2 = 20.0$
Discretisation timestep	$h = 0.005$
Convergence number	$\frac{h}{2}\|\|\boldsymbol{T}\|\|_\infty = 0.0025$

Table 2: Summary of calculation parameters.

No left-moving fields originate from the left end of the beam, and the right-moving fields are calculated by applying the wave splitting transformation (2.3) to the boundary conditions (6.2). In the sequel, the right-moving fields generated by the boundary conditions are referred to as *incoming fields*; meaning that they are incoming on the suspension region $x \in [1, 2]$. At this stage it should also be pointed out that no velocity mode coupling, or transition, occurs at the left end of the beam. The fact that the shear force and the rotation angle both are zero, after the duration of the pulse in the shear force, implies total reflection of the split fields at the left end: a left-moving fast wave arriving at the left end is reflected into a right-moving fast wave of the same functional form. The same holds for a slow wave.

The incoming fields are propagated through the unrestrained region $x \in [0, 1]$ to the reflection boundary. This propagation is carried out by applying the Green's function techniques described in [16]. Thereafter, the reflected fields at $x = 1$ are calculated by using the relation (3.1), together with the numerical solutions of the reflection equation – these are presented in Figures 9 and 10. The reflected fields are then back-propagated to the left end, where total reflection occurs, and forward-propagated once again to the reflection boundary, where a second reflection takes place. This procedure is repeated until all multiple reflections, occurring during a preset time interval, have been taken into account. The total split fields at the reflection boundary are then transformed back to the physical dependent variables by using the inverse wave splitting transformation. The resulting vertical displacement and shear force are shown in Figure 7, for a varying ratio of the length of the viscoelastic suspension to the beam width. The corresponding rotation angle and the bending moment are given in Figure 8 [4]. In the unrestrained case, *i.e.* a free beam, this scattering problem was treated in [16], and the case where the suspension is semi-infinite was treated in [6]. These results are reproduced here to enable a comparison with the finite suspension solution presented here.

The datum of non-dimensional time presented in the figures is taken from the physical arrival time of the incoming fast wave at the reflection boundary. The arrival of the slow wave, at time $s = 0.75$, can be clearly seen in the displacement and the shear force Figure 7. The influence of the fast wave, arriving at time $s = 0$, on the displacement and the shear force is very small and for that reason the main effects of multiple scattering are present from time $s = 4.25$; this is the arrival time of the part of the incoming slow wave that has been once reflected into a slow wave and arrives again at the reflection boundary as a slow wave,

[4] The radius of gyration, r_0, used in this figure is defined in (A.8).

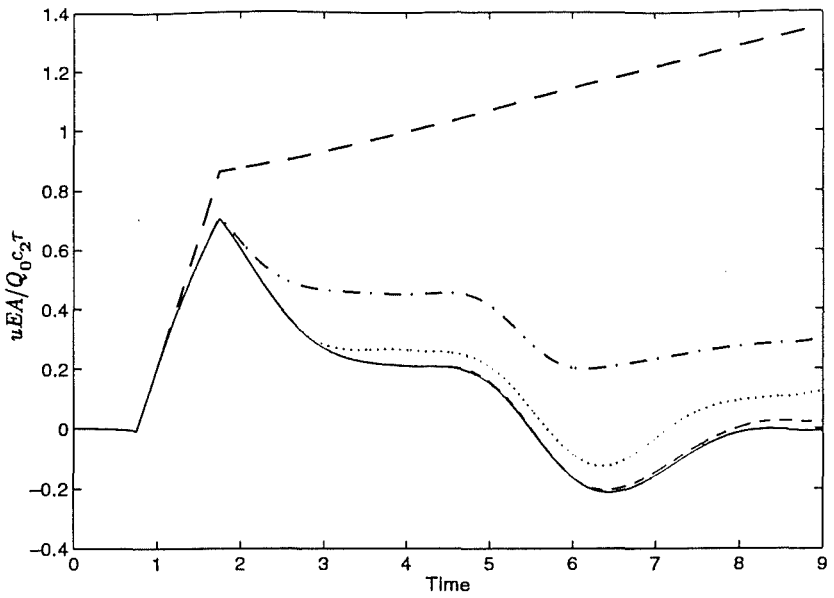

(a) The vertical displacement $u(1, s)$.

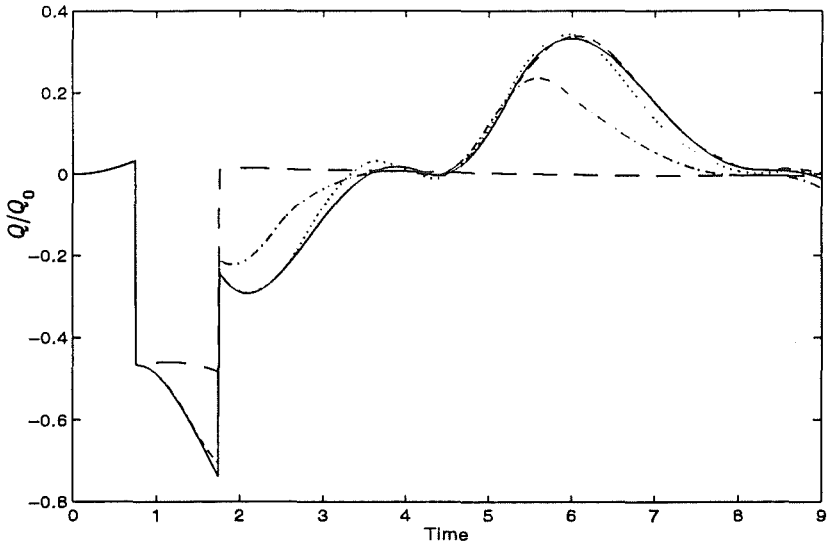

(b) The shear force $Q(1, s)$.

Figure 7: The curves represent beams with five different suspensions: Unrestrained beam: $d = 0$ — — , Semi-infinite: $d \to \infty$ ——— , Finite extent $\frac{d}{a}$ – – – – – – (Note this solution is almost coincident with the semi-infinite case) , Finite extent $\frac{d}{2a}$ ····· , Finite extent $\frac{d}{5a}$ – · – · – .

after total reflection at the left end of the beam. Note that, in the case of the unrestrained beam, the displacement does not approach zero since the free beam is unsupported. Moreover, the limit of the solutions of the finite suspension case, as $d \to 0$, does not coincide with the solutions of the unrestrained case since a support still exists. However, in the limit case $d \to 0$ and $k_i \to 0$ the support will vanish and the unrestrained solutions will be approached. Finally, the change of shape of the shear wave, from the incident one, in the solutions corresponding to the unrestrained beam, is due only to dispersion [16]; similar dispersive effects are apparent in the other cases.

The bending angle and the bending moment, Figure 8, are influenced by both the fast and the slow wave; therefore the effects of multiple reflection appear from time $s = 2.0$. This value of s is the arrival time of the part of the incoming fast wave, that has been once reflected into a fast wave and which arrives again at the reflection boundary as a fast wave, after total reflection at the left end of the beam. In particular, the arrival times of the respective incoming waves are clearly visible in the discontinuities of the time derivative of the bending moment; the incoming fast wave arrives at time $s = 0$, and ends at $s = B$, while the incoming slow wave arrives at time $s = A$ and ends at time $s = C$. As can be seen from this figure, both types of wave have a time duration of 1, which is the time duration of the applied pulse.

The effects of the finite length of the viscoelastic suspension is obvious from Figures 7 and 8. However, note that even in the case where the thickness is one half of the ratio d/a. the solutions are very close to the semi-infinite one. The reason for this is that the effects of the back end of the suspension are heavily damped before reaching the reflection boundary, and therefore have little influence on the solutions of the scattering problem if the ratio d/a is large enough. The jumps in the time derivatives across the respective characteristic traces can be calculated, from equations (3.2), to be

$$[\partial_s R_{11}]_{s=d_3^-}^{s=d_3^+} = \Big(\frac{\gamma d}{2c_2\tau}\Big)^2 k_1 \exp\Big(-\frac{d}{c_2\tau} d_3(x)\Big),$$

$$[\partial_s R_{12}]_{s=d_2^-}^{s=d_2^+} = \frac{\gamma}{2(1+\gamma)}\Big(\frac{d}{c_2\tau}\Big)^2 (\gamma k_1 + k_2) \exp\Big(-\frac{d}{c_2\tau} d_2(x)\Big),$$

$$[\partial_s R_{21}]_{s=d_2^-}^{s=d_2^+} = 0,$$

$$[\partial_s R_{22}]_{s=d_1^-}^{s=d_1^+} = -\Big(\frac{d}{2c_2\tau}\Big)^2 k_2 \exp\Big(-\frac{d}{c_2\tau} d_1(x)\Big),$$

where k_i are the non-dimensional spring constants. It is observed from these equations that the discontinuities decrease exponentially as $x \to 0$. In these equations the square brackets are used to denote the finite jump discontinuities with respect to the variable used in the limits, *i.e.*

$$[f(s)]_{s_1}^{s_2} = f(s_2) - f(s_1).$$

The exponential decay explains why the effects from the reflection, from the back end of the suspension, are damped as they reach the reflection boundary at $x = 0$.

An interpretation of the elements of the reflection kernel is provided. The reflection kernel, $\mathbf{R}(x, s)$, is the part of the impulse response associated with the left-going wave from the inhomogeneous beam region, evaluated at the left boundary x. The reflection kernels R_{11}

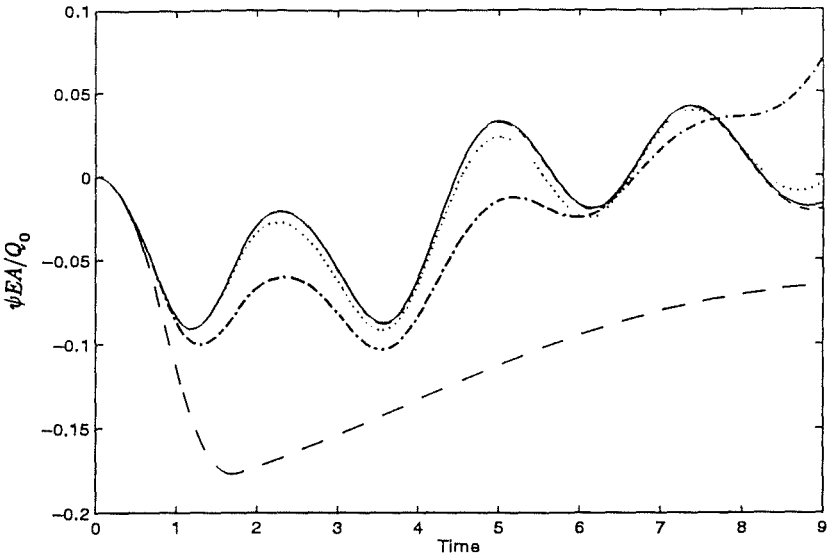

(a) The rotation angle $\psi(1, s)$.

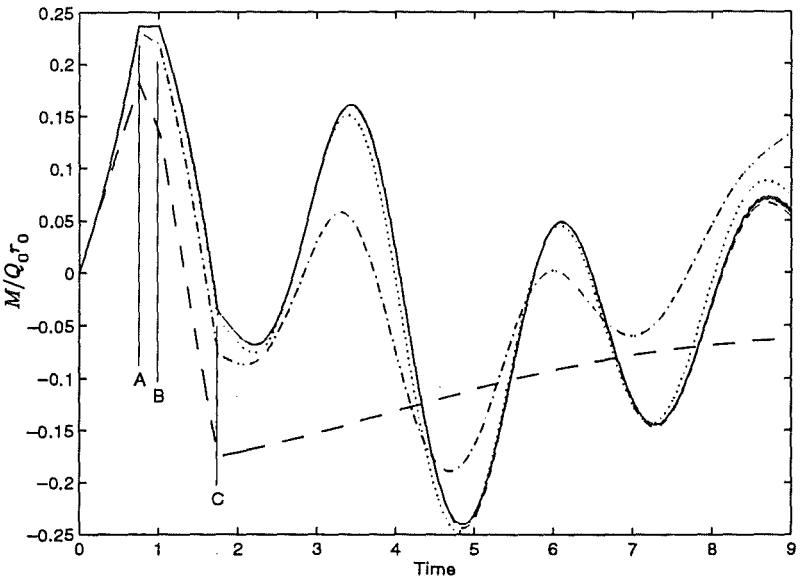

(b) The bending moment $M(1, s)$.

Figure 8: The curves represent beams with five different suspensions: Unrestrained beam: $d = 0$ — — , Semi-infinite: $d \to \infty$ ——— , Finite extent $\frac{d}{a}$ – – – – – – (Note this solution is almost coincident with the semi-infinite case) , Finite extent $\frac{d}{2a}$ ····· , Finite extent $\frac{d}{5a}$ – · – · – .

and R_{21} are the responses caused by impulse excitation in the v_1^+ field, which propagates with the effective shear velocity c_1. Hence, if the excitation at x is

$$\boldsymbol{v}^+ = \begin{bmatrix} \delta(s) \\ 0 \end{bmatrix},$$

then the response is

$$\begin{bmatrix} v_1^-(x,s) \\ v_2^-(x,s) \end{bmatrix} = \begin{bmatrix} R_{11}(x,s) \\ R_{21}(x,s) \end{bmatrix}.$$

Here, R_{11} is the part reflected into a c_1-wave, and R_{21} the part converted into a c_2-wave. Therefore the term R_{21} represents mode conversion. Likewise, R_{12} and R_{22} are the responses due to impulse excitation in the v_2^+ field, propagating with the rod velocity c_2. Hence, if the excitation is

$$\boldsymbol{v}^+ = \begin{bmatrix} 0 \\ \delta(s) \end{bmatrix},$$

then the response is

$$\begin{bmatrix} v_1^-(x,s) \\ v_2^-(x,s) \end{bmatrix} = \begin{bmatrix} R_{12}(x,s) \\ R_{22}(x,s) \end{bmatrix}.$$

R_{22} is the part reflected into a c_2-wave, and R_{12} the part converted into a c_1-wave. Again, the off-diagonal term R_{12} represents mode conversion. The physical reflection kernel of the whole suspension region is $\mathbf{R}(0,s)$.

Up to the time taken for the fast wave to complete the first round trip, reflection effects from the back-wall of the inhomogeneity have not yet reached the left boundary. Therefore, up to non-dimensional time $s = 2(1-x)$, the reflection kernel is spatially invariant. When observing the response at the front-wall, $x = 0$, for the Poisson's ratio used here, the back-wall effects the fast mode R_{22} at time $s = 2$, the mixed modes R_{12} and R_{21} at time $s = 2.75$, and the slow mode R_{11} at $s = 3.50$. However, all these impulse responses are in fact x-dependent after the round trip of the fast mode, R_{22}, due to mode conversion. The spatial invariance of the viscoelastic damping cases, up to the time of the first round trip, can be seen from Figures 9 and 10 where the reflection kernels are plotted with the ratio of the suspension length to the beam width as a parameter. The discontinuities in the time derivatives, at the initial time, can be calculated from equations (3.2), to be

$$[\partial_s R_{11}]_{s=0^-}^{s=0^+} = -\left(\frac{\gamma d}{2c_2\tau}\right)^2 k_1,$$

$$[\partial_s R_{12}]_{s=0^-}^{s=0^+} = -\frac{\gamma}{2(1+\gamma)}\left(\frac{d}{c_2\tau}\right)^2 (\gamma k_1 + k_2),$$

$$[\partial_s R_{21}]_{s=0^-}^{s=0^+} = 0,$$

$$[\partial_s R_{22}]_{s=0^-}^{s=0^+} = \left(\frac{d}{2c_2\tau}\right)^2 k_2.$$

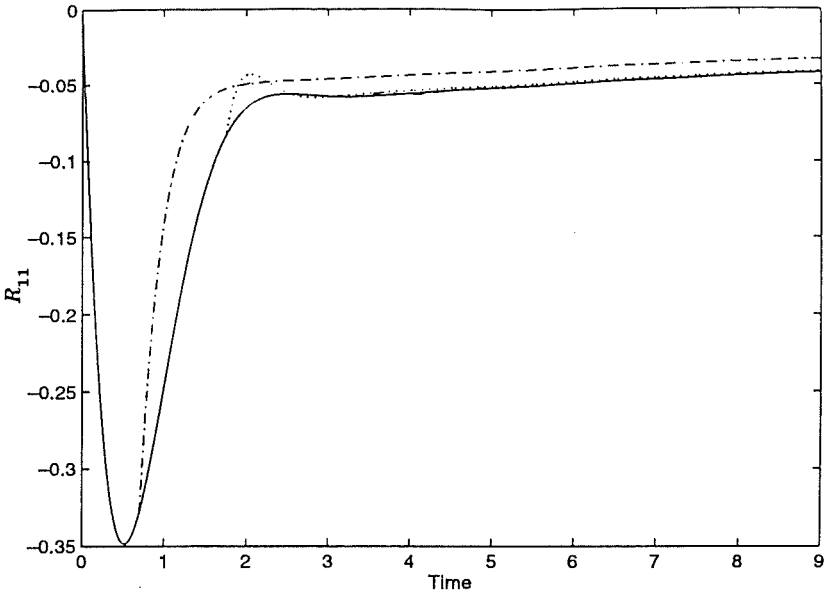

(a) The reflection kernel R_{11}.

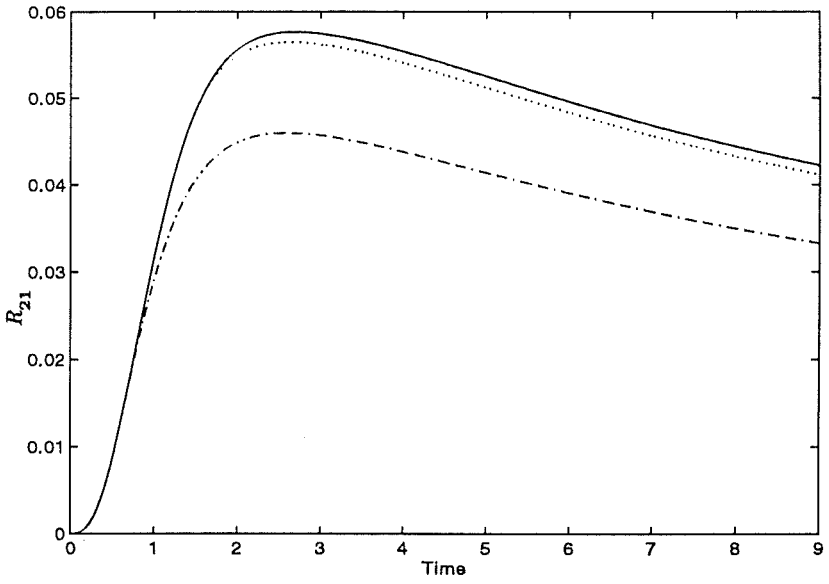

(b) The reflection kernel R_{21}.

Figure 9: The curves represent beams with four different suspensions: Semi-infinite: $d \to \infty$ ——— , Finite extent $\frac{d}{a}$ – – – – – – , Finite extent $\frac{d}{2a}$ ····· , Finite extent $\frac{d}{5a}$ – · – · – .

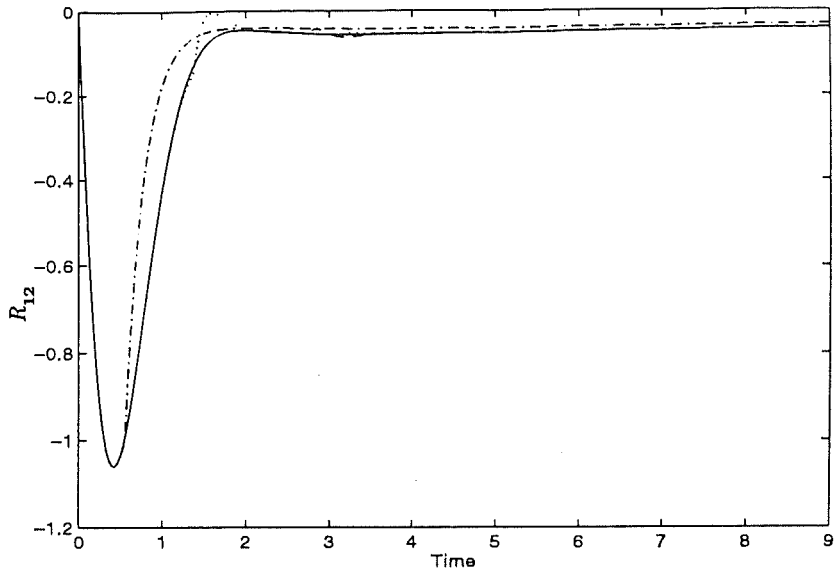

(a) The reflection kernel R_{12}.

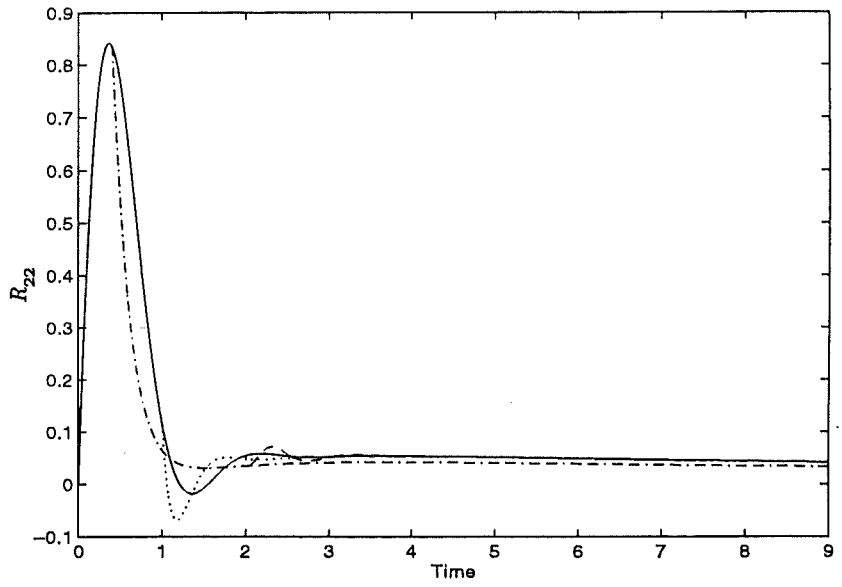

(b) The reflection kernel R_{22}.

Figure 10: The curves represent beams with four different suspensions: Semi-infinite: $d \to \infty$ ——— , Finite extent $\frac{d}{a}$ – – – – – – , Finite extent $\frac{d}{2a}$ ····· , Finite extent $\frac{d}{5a}$ – · – · – .

7 Concluding remarks

The solution of the three-speed reflection equation has proved to be a difficult problem since investigators first examined the matrix-valued reflection kernel [14]. This paper presents a new time-domain algorithm for solving the reflection equation associated with scattering on the Timoshenko beam. The algorithm consists of a predictor-corrector iterator combined with the method of characteristics and linear interpolation in the spatial coordinate.

The algorithm has been applied to solve a direct wave scattering problem from a finite suspension of a Timoshenko beam. Some numerical examples of the method have been presented and it has been illustrated that our method provides a useful tool in examination of the wave scattering properties of the suspension region. These examples show that for the reflection problem the suspension can be treated as semi-infinite, at least when $d/a > 0.3$.

The construction of the numerical algorithm for the finite suspension case provides for the future extension of this work: to augment the numerical algorithm to cover the inhomogeneous beam, thus including the possibility of longitudinally varying material parameters. Then the inverse problem of recovering a geometrical variation of the beam, from knowledge of boundary data, can be considered. Furthermore, numerical solutions of the reflection equation are needed when numerical solution of the transmission problem is addressed, since the reflection kernel appears as a source term in the equation for the transmission kernel [6].

Acknowledgement

Professor Peter Olsson at the Division of Mechanics is thanked for many useful discussions during the realisation of this work. This paper is partially supported by a grant from The Swedish Research Council for Engineering Sciences, which is gratefully acknowledged.

References

[1] Ingegerd Åberg, Gerhard Kristensson, and David J.N. Wall. Propagation of transient electromagnetic waves in time-varying media — direct and inverse scattering problems. *Inverse Problems*, 11(1):29–49, 1995.

[2] Ingegerd Åberg, Gerhard Kristensson, and David J.N. Wall. Transient waves in non-stationary media. *J. Math. Phys.*, 37(5):2229–2252, 1996.

[3] E. Ammicht, J.P. Corones, and R.J. Krueger. Direct and inverse scattering for viscoelastic media. *J. Acoust. Soc. Am.*, 81:827–834, 1987.

[4] I.S. Ayoubi. Numerical solution of the inverse scattering problem for hyperbolic systems of N-components in semi-infinite media. In J.P. Corones, G. Kristensson, P. Nelson, and D.L. Seth, editors, *Invariant Imbedding and Inverse Problems*, pages 187–208, Philadelphia, 1992. SIAM.

[5] R.S. Beezley and R.J. Krueger. An electromagnetic inverse problem for dispersive media. *J. Math. Phys.*, 26(2):317–325, 1985.

[6] D.V.J. Billger and P.D. Folkow. The imbedding equations for the Timoshenko beam. *Accepted for publication in the Journal of Sound and Vibration.*

[7] T.J. Connolly and D.J.N. Wall. On some inverse problems for a nonlinear transport equation. *Inverse Problems*, 13(2):283–295, 1997.

[8] J.P. Corones, M.E. Davison, and R.J. Krueger. Direct and inverse scattering in the time domain via invariant imbedding equations. *J. Acoust. Soc. Am.*, 74(5):1535–1541, 1983.

[9] J.P. Corones, M.E. Davison, and R.J. Krueger. Wave splittings, invariant imbedding and inverse scattering. In A.J. Devaney, editor, *Inverse Optics, Proceedings of the SPIE*, pages 102–106, SPIE Bellingham, WA, 1983. Proc. SPIE 413.

[10] J.P. Corones and A. Karlsson. Transient direct and inverse scattering for inhomogeneous viscoelastic media: obliquely incident SH mode. *Inverse Problems*, 4:643–660, 1988.

[11] J.P. Corones, G. Kristensson, P. Nelson, and D.L. Seth, editors. *Invariant Imbedding and Inverse Problems*, Philadelphia, 1992. SIAM. Symposium held in Albuquerque, April 1990.

[12] J.P. Corones and R.J. Krueger. Obtaining scattering kernels using invariant imbedding. *J. Math. Anal. Appl.*, 95:393–415, 1983.

[13] G.R. Cowper. The Shear Coefficient in Timoshenko's Beam Theory. *Journal of Applied Mechanics*, pages 335–340, June 1966.

[14] R.P. Dougherty. *Direct and inverse scattering of classical waves at oblique incidence to stratified media via invariant imbedding equations.* PhD thesis, Iowa State University, Ames, Iowa, 1986.

[15] P.D. Folkow. Time domain inversion of the spatially invariant reflection equation of the Timoshenko beam. Technical Report 1996:4, Division of Mechanics, Chalmers University of Technology, 1996.

[16] P.D. Folkow, G. Kristensson, and P. Olsson. Time domain Green functions for the homogeneous Timoshenko beam. *Accepted for publication in Quart. J. Mech. Appl. Math.*

[17] A. Karlsson. Inverse scattering for viscoelastic media using transmission data. *Inverse Problems*, 3:691–709, 1987.

[18] A. Karlsson. Wave propagators for transient waves in one-dimensional media. *Wave Motion*, 24:85–99, 1996.

[19] A. Karlsson and K Kreider. Transient electromagnetic wave propagation in transverse periodic media. *Wave Motion*, 23:259–277, 1996.

[20] A. Karlsson and R. Stewart. Wave propagators for transient waves in periodic media. *J. Opt. Soc. Am. A*, 12(9):1513–1521, 1995.

[21] G. Kristensson. Direct and inverse scattering problems in dispersive media—Green's functions and invariant imbedding techniques. In R. Kleinman, R. Kress, and E. Martensen, editors, *Direct and Inverse Boundary Value Problems*, Methoden und Verfahren der Mathematischen Physik, Band 37, pages 105–119, Frankfurt am Main, 1991. Peter Lang.

[22] Gerhard Kristensson and David J.N. Wall. Direct and inverse scattering for transient electromagnetic waves in nonlinear media. Technical Report 153/1-23/(1997), Canterbury University, Christchurch 1, New Zealand, 1997.

[23] R.J. Krueger and R.L. Ochs, Jr. A Green's function approach to the determination of internal fields. *Wave Motion*, 11:525–543, 1989.

[24] P. Linz. *Theoretical Numerical Analysis: An Introduction to Advanced Techniques.* Wiley-Interscience, New York, 1979.

[25] P. Olsson and G. Kristensson. Wave splitting of the Timoshenko beam equation in the time domain. *Zeitschrift für andgewandte Mathematik und Physik*, 45:866–881, 1994.

[26] R.D. Stewart. *Transient electromagnetic scattering on anisotropic media.* PhD thesis, Iowa State University, Ames, Iowa, 1989.

[27] Z. Sun and G. Wickham. The inversion of transient reflection data to determine solid grain structure. *Wave Motion*, 18:143–162, 1993.

[28] S.P. Timoshenko. On the correction for shear of the differential equation for transverse vibrations of prismatic bars. *Phil. Mag.*, XLI:744–746, 1921. Reprinted in The Collected Papers of Stephen P. Timoshenko, McGraw-Hill, London 1953.

[29] C.R. Vogel. Wave splitting for some nonhyperbolic time-dependent pdes. In J.P. Corones, G. Kristensson, P. Nelson, and D.L. Seth, editors, *Invariant Imbedding and Inverse Problems.* SIAM, 1992.

[30] David J.N. Wall and Peter Olsson. Invariant imbedding and hyperbolic heat waves. *J. Math. Phys.*, 38(3):1723–1749, 1997.

[31] D.J.N. Wall. On the numerical solution of a functional differential equation pertaining to a wave equation. In P. Nelson J.P. Corones, G Kristensson and D.L. Seth, editors, *Invariant Imbedding and Inverse Problems*, pages 169–186, Philadephia, 1992. SIAM.

A Operators originating from the wave splitting transformation

For completeness this appendix presents important operators and functions referred to in this paper. The functions $F_i(t)$ and the matrix elements $A_{ij}(t)$, throughout the paper, are all non-dimensional in accordance with the travel time transformation. However, for notational convenience, the notation in this appendix assumes real time t. All temporal convolutions are therefore also considered in real time. The results however, are easily transformed with a simple substitution of variables $t = sd/c_2$.

The kernel functions $F_i(t)$ that originate from the wave splitting transformation can be

written

$$\begin{aligned} F_1(t) &= H(t)\sum_{k=1}^{\infty}\frac{\Gamma(3/2)}{k!\Gamma(3/2-k)}(-1)^k(q+1)^{-k}W_k(t/\tau), \\ F_2(t) &= H(t)\sum_{k=1}^{\infty}\frac{\Gamma(3/2)}{k!\Gamma(3/2-k)}(q-1)^{-k}W_k(t/\tau), \end{aligned} \tag{A.1}$$

where $H(t)$ is the Heaviside step function, Γ the gamma function and $W_k(\xi)$ are integrals of modified Bessel functions

$$W_k(\xi) = \partial_\xi^{-k+1}\frac{kI_k(\xi)}{\xi}, \qquad \partial_\xi^{-1}f(\xi) = \int_0^\xi f(\xi')\,d\xi'.$$

The characteristic time τ is defined as

$$\tau = \frac{1}{2c_1}\left(1-\frac{c_1^2}{c_2^2}\right)\sqrt{\frac{f_2}{f_1}}, \tag{A.2}$$

and q represents the following ratio

$$q = \frac{c_2^2+c_1^2}{c_2^2-c_1^2}.$$

In order to simplify the numerical treatment, these functions may be expanded in a power series

$$F_i(t) = H(t)\sum_{k=0}^{\infty}a_{i,k}t^{2k}.$$

However, for large arguments it is advantageous to represent eq. (A.1) asymptotically. Since $W_k(\xi)$ are of exponential order $1/\tau$ it follows that

$$F_i(t) \approx e^{t/\tau}\sum_{k=1}^{\infty}b_{i,k}t^{-(2k+1)/2}.$$

Schemes for computing the coefficients $a_{i,k}$ and $b_{i,k}$ are described in [25].

The elements A_{ij} of the matrices $\mathbf{A}_i$, appearing in (3.9), are expressed in terms of the function Q, defined in (A.7), and its derivative $\partial_t Q$ through

$$A_{ij} = \frac{1}{c_2}e^{-t/\tau}\left(a_{ij}\partial_t Q + b_{ij} * Q\right), \tag{A.3}$$

where the constants a_{ij} and the functions $b_{ij}(t)$ are defined as

$$
\begin{aligned}
a_{11} &= \frac{c_1^2 - c_2^2}{c_1 c_2^2}, \qquad a_{12} = a_{21} = 0, \qquad a_{22} = \frac{c_1^2 - c_2^2}{c_1^2 c_2}, \\
b_{11} &= \frac{c_1}{c_2}\left(\frac{\partial_t S}{c_2} + F_2 + S * F_2\right) - F_1, \\
b_{12} &= \frac{c_1}{c_2}\left(\frac{\partial_t S}{c_1} + F_1 + S * F_1\right) - F_2, \\
b_{21} &= \left(\frac{c_1^2}{c_2^2 r_0^2} - \frac{1}{2 r_0 c_2 \tau}\right)\left(\frac{\partial_t U}{c_1} + F_1 * U\right) - \frac{1}{c_1}\partial_t U * V - F_1 * U * V, \\
b_{22} &= \left(\frac{1}{r_0^2} + \frac{1}{2 r_0 c_2 \tau}\right)\left(\frac{\partial_t U}{c_2} + F_2 * U\right) + \frac{1}{c_2}\partial_t U * V + F_2 * U * V + \left(1 - \frac{c_2^2}{c_1^2}\right) F_2.
\end{aligned}
\tag{A.4}
$$

The transformation matrices $\mathcal{P}$ and $\mathcal{P}^{-1}$ can be represented as

$$
\mathcal{P} = \mathcal{Q}\begin{bmatrix}
-\left(\lambda_2^2 - c_1^{-2}\partial_t^2\right) & -\lambda_1 & \mathcal{S}\lambda_2 - \lambda_1 & 1 \\
\lambda_1^2 - c_1^{-2}\partial_t^2 & \lambda_2 & -\left(\mathcal{S}\lambda_1 - \lambda_2\right) & -1 \\
-\left(\lambda_2^2 - c_1^{-2}\partial_t^2\right) & \lambda_1 & -\left(\mathcal{S}\lambda_2 - \lambda_1\right) & 1 \\
\lambda_1^2 - c_1^{-2}\partial_t^2 & -\lambda_2 & \mathcal{S}\lambda_1 - \lambda_2 & -1
\end{bmatrix},
\tag{A.5}
$$

$$
\mathcal{P}^{-1} = \begin{bmatrix}
1 & 1 & 1 & 1 \\
-\lambda_1\left(1 - \mathcal{U}\lambda_2^2\right) & -\lambda_2\left(1 - \mathcal{U}\lambda_1^2\right) & \lambda_1\left(1 - \mathcal{U}\lambda_2^2\right) & \lambda_2\left(1 - \mathcal{U}\lambda_1^2\right) \\
-\lambda_1 \mathcal{U}\lambda_2^2 & -\lambda_2 \mathcal{U}\lambda_1^2 & \lambda_1 \mathcal{U}\lambda_2^2 & \lambda_2 \mathcal{U}\lambda_1^2 \\
\lambda_1^2 - c_1^{-2}\partial_t^2 & \lambda_2^2 - c_1^{-2}\partial_t^2 & \lambda_1^2 - c_1^{-2}\partial_t^2 & \lambda_2^2 - c_1^{-2}\partial_t^2
\end{bmatrix}.
\tag{A.6}
$$

$\mathcal{Q}$, $\mathcal{U}$ and $\mathcal{S}$ act as convolution operators

$$
\begin{aligned}
\mathcal{Q} f(t) &= \big(Q(\cdot) * f(\cdot)\big)(t), \\
\mathcal{U} f(t) &= \big(U(\cdot) * f(\cdot)\big)(t), \\
\mathcal{S} f(t) &= \frac{c_1}{c_2}\Big(f(t) + \big(S(\cdot) * f(\cdot)\big)(t)\Big),
\end{aligned}
\tag{A.7}
$$

where

$$
\begin{aligned}
Q(t) &= \frac{r_0 c_2}{4} H(t) \int_0^{t/\tau} I_0(\xi)\, d\xi, \\
U(t) &= \frac{r_0 c_2^2}{c_1} H(t) \sin\left(\frac{c_1 t}{r_0}\right), \\
S(t) &= \frac{c_1}{r_0} H(t) \int_0^{c_1 t / r_0} \frac{J_1(\xi)}{\xi}\, d\xi.
\end{aligned}
$$

Here, r_0 is the radius of gyration defined by

$$
r_0 = \sqrt{\frac{I}{A}} = \frac{c_1}{c_2}\sqrt{\frac{f_2}{f_1}}.
\tag{A.8}
$$

Furthermore, the operator $\mathcal{Q}$ satisfies

$$2\mathcal{Q}\left(\lambda_1^2 - \lambda_2^2\right) = 1.$$

The λ_i are the of the wave splitting transformation. Formally squaring these yields

$$\lambda_1^2 = \frac{1}{c_1^2}\frac{\partial^2}{\partial t^2} - \frac{1}{2r_0c_2\tau} - V(\cdot)*,$$

$$\lambda_2^2 = \frac{1}{c_2^2}\frac{\partial^2}{\partial t^2} + \frac{1}{2r_0c_2\tau} + V(\cdot)*,$$

where the function $V(t)$ is written

$$V(t) = \frac{1}{r_0c_2\tau t}H(t)I_2(t/\tau).$$

As pointed out in [16], this corrects an error in λ_i^2 from [25].

B Approximation of convolution integrals

The convolution integrals are approximated by using the trapezoidal rule on the uniform partition, $s_k - s_{k-1} = h$, of the range $s \in [0, s_k]$ in the integration. Let $\mathbf{A}$ and $\mathbf{B}$ denote general 2-by-2 matrix functions, then the convolution product

$$(\mathbf{A} * \mathbf{B})_{ij}(s_k) = \int_0^{s_k} A_{im}(s')B_{mj}(s_k - s')\,ds', \tag{B.1}$$

is approximated as

$$(\mathbf{A} * \mathbf{B})_{ij,k} = h\sum_{p=0}^{k} A_{im,p}B_{mj,k-p} - \frac{h}{2}\left(A_{im,0}B_{mj,k} + A_{im,k}B_{mj,0}\right) + \mathcal{O}\left(h^2\right).$$

In matrix form this reads, to a discretisation error of $\mathcal{O}\left(h^2\right)$,

$$(\mathbf{A} * \mathbf{B})_k = h\sum_{p=0}^{k} \mathbf{A}_p\mathbf{B}_{k-p} - \frac{h}{2}\left(\mathbf{A}_0\mathbf{B}_k + \mathbf{A}_k\mathbf{B}_0\right). \tag{B.2}$$

By applying (B.2) twice to the double convolution, along with the fact that $(\mathbf{A} * \mathbf{B})_0 \equiv 0$, it follows

$$\begin{aligned}(\mathbf{A} * \mathbf{B} * \mathbf{A})_k &= h\sum_{p=0}^{k} (\mathbf{A} * \mathbf{B})_p\,\mathbf{A}_{k-p} - \frac{h}{2}\left((\mathbf{A} * \mathbf{B})_0\,\mathbf{A}_k + (\mathbf{A} * \mathbf{B})_k\,\mathbf{A}_0\right)\\ &= h\sum_{p=1}^{k}\left(h\sum_{q=0}^{p}\mathbf{A}_q\mathbf{B}_{p-q} - \frac{h}{2}\left(\mathbf{A}_0\mathbf{B}_p + \mathbf{A}_p\mathbf{B}_0\right)\right)\mathbf{A}_{k-p}\\ &\quad - \frac{h}{2}\left(h\sum_{p=0}^{k}\mathbf{A}_p\mathbf{B}_{k-p} - \frac{h}{2}\left(\mathbf{A}_0\mathbf{B}_k + \mathbf{A}_k\mathbf{B}_0\right)\right)\mathbf{A}_0, \qquad k \in \mathbb{Z}_+.\end{aligned}$$

Finally, to a discretisation error of $\mathcal{O}(h^2)$,

$$
\begin{aligned}
(\mathbf{A} * \mathbf{B} * \mathbf{A})_k = h^2 \sum_{p=1}^{k} \sum_{q=0}^{p} \mathbf{A}_q \mathbf{B}_{p-q} \mathbf{A}_{k-p} \\
- \frac{h^2}{2} \sum_{p=1}^{k} (\mathbf{A}_0 \mathbf{B}_p \mathbf{A}_{k-p} + \mathbf{A}_p \mathbf{B}_0 \mathbf{A}_{k-p} + \mathbf{A}_p \mathbf{B}_{k-p} \mathbf{A}_0) \\
+ \frac{h^2}{4} (\mathbf{A}_k \mathbf{B}_0 \mathbf{A}_0 - \mathbf{A}_0 \mathbf{B}_k \mathbf{A}_0), \qquad k \in \mathbb{Z}_+.
\end{aligned}
$$